Dispersion of heavy particles under sea waves ⊘

A. De Leo ⓘ ; A. Stocchino ✉ ⓘ

Check for updates

View Online

Export Citation

Articles You May Be Interested In

Efficiency of energy and enstrophy transfers in periodical flows

Physics of Fluids (April 2023)

Horizontal and vertical dispersion in a wind-driven oceanic gyre model

Physics of Fluids (October 2024)

Particle dynamics due to interaction between a breaking-induced vortex and a nearbed vortex

Physics of Fluids (January 2023)

Dispersion of heavy particles under sea waves

View Online   Export Citation   CrossMark

A. De Leo[1] (iD) and A. Stocchino[2,3,a)] (iD)

AFFILIATIONS

[1]DICCA, Dipartimento di Ingegneria Civile, Chimica e Ambientale, Università degli Studi di Genova, 16145 Genova, Italy
[2]Department of Civil and Environmental Engineering, Hong Kong Polytechnic University, Hung Hom, Kowloon 999077, Hong Kong
[3]State Key Laboratory of Marine Pollution, City University of Hong Kong, 83 Tat Chee Avenue, Kowloon 999077, Hong Kong

[a)]Author to whom correspondence should be addressed: alessandro.stocchino@polyu.edu.hk

ABSTRACT

We report the results of a series of numerical simulations performed with the aim to describe the dispersion of heavy particles transported by sea waves. Recent studies investigated the interplay between the wave Stokes drift and the inertial character of negatively buoyant particles that, ultimately, yields an augmented settling velocity. Our interest is to investigate the possible occurrence of a Brownian regime that would allow for the definition of a diffusion coefficient. The velocity and acceleration auto-correlation functions and the corresponding integral time scales show that already at a very low Stokes number the particles behave very differently from the fluid. The main consequence is that an asymptotic diffusive regime is rarely observed, except as a transient regime or when the background random noise is comparable with the wave field velocities.

Published under an exclusive license by AIP Publishing. https://doi.org/10.1063/5.0074760

I. INTRODUCTION

The transport of heavy particles has attracted the attention of scientists in the last decades, owing to the wide range of applications in both industrial and environmental flows. A great effort has been dedicated to understand how homogeneous turbulence or turbulent boundary layers are able to transport particles at different scales. The inertial character of the particles proved to modify substantially the statistics of the particle velocity and acceleration fluctuations[1–3] and the shape of the auto-correlation functions and the corresponding integral scales.[4–6] One of the interesting consequences of the modified velocity auto-correlation functions is the effect on the dispersion regimes that heavy particles show.[6–8]

Fluid particles immersed in a turbulent flow tend to behave differently from their fluid counterpart, and this is often investigated using the auto-correlation functions and the flow properties of the *fluid seen by particles*.[7,9–11] Inertial particles were found to behave differently from fluid particles already for Stokes number of order one, and their typical Lagrangian integral scales are extremely sensitive to the values of the Stokes number.[7] A great amount of studies are dedicated to the interaction of heavy particles and turbulent flows (boundary layers or homogeneous turbulence and channel flows showing interesting processes of clustering[12–16]).

Gravity effects on heavy particles transport have received less attention, even if they play a determinant role in several geophysical contexts, e.g., in atmospheric transport.[15,17–21] One of the main results

of the mentioned studies is that the diffusion theory by Taylor[22] proved to be valid, provided a correct definition of the decorrelation time is used, even for fairly high values of the Stokes number. In particular, a diffusive regime was observed numerically and experimentally, leading to diffusion coefficients that can be lower or higher with respect to the fluid ones depending on the Stokes number.[7,17] A theoretical generalization of Taylor's formula for inertial particles, non-interacting among themselves, carried by a general flow was recently proposed.[23] After introducing a wide class of models of inertial particle dynamics, the authors analyzed several particular cases, starting from the Basset–Buossinesq–Oseen equation and the Maxey–Riley equation[24] to describe the inertial particle trajectories and the resulting Taylor's formulas in simplified cases (buoyancy-force case, Brownian force case, limiting cases for the Stokes number).

Only recently, the transport of inertial particles under the action of sea waves received attention.[25–29] These studies showed that heavy particles transported by Stokes drift, generated by sea waves, ultimately reach an increased settling velocity with respect to the still fluid settling. Heavy particles tend to settle following looping trajectories, which quite soon differ from the fluid particle ones. All the above studies, however, did not deepen the dispersion process related to this form of transport, except a mention of longitudinal dispersion in DiBenedetto *et al.*[26]

The importance of a thorough investigation of the dispersion of heavy particles resides in the application to microplastic transport,

03 February 2025 01:01:57

which is nowadays considered one of the major threats for the marine environments.[30–32] Note that microplastic, defined as plastic debris with dimension less than 5 mm, can be either lighter or heavier than sea water.[33] In fact, the mass density depends primarily on the plastic composition, with a wide range of values (e.g., high density polyethylene, 930–970 kg m^{-3}, polypropylene, 850–920 kg m^{-3}, polyvinyl chloride, 1300–1450 kg m^{-3}). Moreover, plastic debris exposed to sea water and sunlight are subject to bio-film growth of several kinds (bacteria and algae bio-accumulation) that ultimately could increase the mass density.[34] Moreover, it was demonstrated that several noxious substances, e.g., heavy metals, can be accumulated in the biofilm and transported over long distances.[35]

It is of great importance understanding whether the transport of heavy particles by sea waves, relevant especially in coastal zones, can be described in terms of a diffusive process. In fact, the existence of an asymptotic diffusive regime would allow for a Fickian-like closure for the mass flux through a diffusion coefficient. So far, most of the numerical models adopted to simulate the fate of microplastic debris rely on the assumption that small plastic particles are neutrally buoyant. Only a few models implement other approaches allowing to consider a settling velocity disregarding any drag-induced effect, both in a Lagrangian[36,37] and in an Eulerian[37] framework, assuming a diffusion process for the plastic particles.

The main goal of the present study is to investigate the possibility that the transport of inertial particles owing to sea waves could be described in terms of an asymptotic diffusive regime. We build a simplified transport model based on the Maxey and Riley's equations,[24] including the effect of background random flow disturbances superimposed to the wave field. The inclusion of a stochastic term proportional to a diffusion coefficient is a common simplified model to consider an isotropic random force acting on the particle.[23,38,39] The main application is the transport of negatively buoyant microplastic particles. The choice of the range of the main particle parameters is guided by several studies of observations of microplastics sampled both in the water column and in the sea bed sediment. In a recent statistical analysis, Kooi and Koelmans[33] analyzed the data from many field studies and provided a description in terms of multi-dimensional probability functions. We rely on the cited work for the definition of the range of particle diameters and the density of the inertial particle. Moreover, sea wave parameters are varied with the aim to understand the role of the intensity of the Stokes drift.

The paper is organized as follows. In Sec. II, a brief description of the mathematical model and the numerical experiments is provided; in Sec. III, the results of our analysis are described and discussed. The main conclusions are reported in Sec. IV.

II. MATHEMATICAL MODEL AND NUMERICAL EXPERIMENTS

The Eulerian wave flow on a vertical plane (x, z), $\mathbf{u}(\mathbf{x}, t) = (u_x(\mathbf{x}, t); u_z(\mathbf{x}, t))$ is calculated assuming a second order Stokes wave as[40]

$$
\begin{cases}
u_x(x,z,t) = \left(\dfrac{gka}{\omega}\right)f_{c1}\cos\left(kx - \omega t\right) + \left(\dfrac{g(ka)^2}{\omega}\right)f_{c2}\cos 2(kx - \omega t), \\[2ex]
u_z(x,z,t) = \left(\dfrac{gka}{\omega}\right)f_{d1}\sin\left(kx - \omega t\right) + \left(\dfrac{g(ka)^2}{\omega}\right)f_{d2}\sin 2(kx - \omega t),
\end{cases}
\tag{1}
$$

where g is the gravitational acceleration, a is the wave amplitude, $k = 2\pi/\lambda$ is the wave number, and λ the wavelength, and $\omega = 2\pi/T$ is the angular frequency with T the wave period. The wavenumber k and the angular frequency ω are linked by a dispersion relation as

$$
\omega = kU_0 + \sigma,
\tag{2}
$$

where U_0 is the value of a possible background uniform current velocity and σ is the frequency of the wave in the moving frame of Ref. 41. For the present analysis, we did not consider any background flow U_0.

The functions f_{c1}, f_{c2}, f_{d1}, and f_{d2} are hyperbolic functions of the water depth h and the vertical coordinate z and read

$$
f_{c1} = \cosh(ks)/\cosh(kz);
\tag{3}
$$

$$
f_{c2} = 3\cosh(2ks)/4\sinh^3(kz)\cosh(kh);
\tag{4}
$$

$$
f_{d1} = \sinh(ks)/\sinh(kz);
\tag{5}
$$

$$
f_{d2} = 3\sinh(2ks)/4\sinh^3(kz)\cosh(kh),
\tag{6}
$$

having defined s as $(h + z)$.

In the following, different waves are described in terms of the wave steepness parameter[27] defined as H/gT^2, where $H = 2a$, or the Froude number $F_r = \omega a/c$, where c is the wave celerity.[25]

The motion of a small spherical inertial particle can be described by a set of equations that reads

$$
\begin{cases}
\dfrac{d\mathbf{x}(t)}{dt} = \mathbf{u}^p(t) + \sqrt{2D}\mathbf{R}(t), \\[2ex]
\dfrac{d\mathbf{u}^p(t)}{dt} = \dfrac{\mathbf{u}(\mathbf{x}, t) - \mathbf{u}^p(t)}{\tau} + (1 - \beta)\mathbf{g} + \beta\dfrac{d\mathbf{u}(\mathbf{x}, t)}{dt},
\end{cases}
\tag{7}
$$

where $\mathbf{u}^p(t)$ is the Lagrangian particle velocity, $\mathbf{u}(\mathbf{x}, t)$ is the flow field acting on the particle derived from Eq. (1), β is the added-mass parameter defined as $\beta = 3\rho_f/(\rho_f + 2\rho_p)$ with ρ_f and ρ_p the fluid density and particle density, respectively, and, finally, τ is the Stokes response time defined as $\tau = d_p^2/(12\beta\nu)$, d_P being the particle diameter and ν the fluid kinematic viscosity. The Stokes number can be readily evaluated as $S_t = \omega\tau$.

This model is a modified version of the original set of equations of Maxey and Riley[24] for a spherical particle. In particular, we neglect the Faxen and Basset terms from the original equations similarly to previous studies.[25–27] Moreover, differently from the original set of equations, in the present context, we included a zeroth-order Markov model term in the first equation. With this simple model, a stochastic noise is added to the particle positions through the term $\mathbf{R}(t)$ that assumes random values with zero mean and unitary variance. The Brownian motion generated is multiplied by a diffusion coefficient D, which should synthetically describe the presence of an external Brownian force per unit mass equal to $\sqrt{2D/\tau}\mathbf{R}(t)$.[23,38] It could also be interpreted as the effect of the unresolved turbulent flow scales on single inertial particles.[39,42,43] In our analysis, the coefficient D is used as a free parameter, varied in a range between the molecular diffusion value (10^{-6} m^2 s^{-1}) and a value of 10^{-1} m^2 s^{-1}. The inclusion of a Brownian term was used in several previous studies focused on the transport of inertial particles or droplets immersed in different flow fields.[23,38,39,42,44,45]

We acknowledge that this is a quite crude representation of the influence of possible small scale turbulence effects. However, the

03 February 2025 01:01:57

particular flow under investigation, namely the flow field generated by a sea wave, is usually characterized by low turbulent intensities, quite different from classical turbulent flows used in other context where the transport of inertial particles has been studied.

The Lagrangian transport equations (7) were numerically solved using a fourth order Runge–Kutta method with a fixed integration time step much smaller than the Stokes time. Care must be taken on the choice of the integration time in order to resolve time scales of the order of τ; in our analysis, we set the integration time as $\Delta t = \tau/30$.

To investigate the possible dispersive regimes, we designed several series of numerical experiments varying the main physical parameters. In particular, four series of experiments were performed varying the wave parameter H/gT^2 in a range between 0.001 and 0.006 ($F_r = 0.02 - 0.12$). All simulations were performed in deep water conditions. For each wave condition, the particle diameter was varied in a range between 10^2 and 10^3 μm maintaining a fixed value of the added-mass parameter β equal to 0.9677. The resulting values of the Stokes number cover a range approximately between 0.0009 and 0.09.

A total of 456 simulations were performed using 3500 numerical particles, released at the free surface, for an integration time equal to 1500–3500 wave periods, depending on S_t. The duration of the simulation is chosen in order to let the particles reach a depth where the Stokes drift is no longer felt. The main parameters of the numerical simulations are reported in Table I.

Finally, it is worth discussing the range of particle parameters used for the present study. Since the main application that stimulated the investigation is the transport of microplastic and the role of the sea wave Stokes drift, we selected the range of particles diameters and the values of the relative density using the data analysis reported in two recent reviews on sampled microplastic debris, namely Hidalgo-Ruz et al.[30] and Kooi and Koelmans.[33]

Hidalgo-Ruz et al.[30] reviewed 68 studies with the aim to summarize the range of particle debris in terms of sizes and densities. Based on similar data sets, Kooi and Koelmans[33] suggested a statistical interpretation of the data using multidimensional probability density functions (pdf) involving size, density, and shapes (Corey shape factor, CSF[46]) of the debris. In particular, the distribution of plastic density is well fitted by a Normal-Inverse Gaussian distribution with a central value of around $1000\,kg/m^3$ and a marked positive skewness with non-negligible probability values up to $1600\,kg/m^3$. From this analysis, almost half of the observed plastic debris has a density in a range between 960 and $1580\,kg/m^3$, see the data of Figs. S1 and S4 and Table S3. Using the range of wave parameters reported in Table I, the Stokes number used for the present numerical experiments well describes a wide range of microplastic debris observed in the field.

We acknowledge that assuming a spherical shape is quite a crude representation of the real microplastic debris, since microplastic debris shows a Corey shape factor distribution dominated by fibers and fragments ($CSF = 0.25 - 0.75$) with a second peak at a CSF of 0.07, which is mainly attributed to sheets.[33]

III. RESULTS AND DISCUSSION
A. Particle trajectories, velocities, and accelerations

Particle trajectories were computed using system (7), and typical examples for a fixed Stokes number ($S_t = 2 \times 10^{-3}$) are shown in Fig. 1 for two wave conditions, $H/gT^2 = 0.001$ and $H/gT^2 = 0.006$, and varying the values of the random term in the equations.

For a very low value of the coefficient D [panels (a) and (d)], the particle trajectories are similar to the one computed in previous studies[25,27] or measured in laboratory experiments.[29] The inertial character of heavy particles, already at a low value of the Stokes number, interacts with the wave Stokes drift leading to an augmented settling velocity. The net settling velocity was experimentally measured and was found to depend on both the particle characteristics and the wave parameter.[29]

Following the theoretical predictions of Santamaria et al.[25] under linear wave approximation, the maximum dimensionless longitudinal distance traveled by the particle owing to the sea waves depends on the added-mass parameter β, the wave Froude number, and the Stokes number. As shown in Fig. 1, the maximum distance in the wave propagation is several wavelengths. Increasing the value of the background random process through the coefficient D leads to, as expected, less regular trajectories, see panels (b), (c), (e), and (f). Note that Fig. 1 shows only one particle trajectory out of the 3500 particles used.

For the present purpose, the velocities and acceleration time signals of the particle and the *fluid seen by particle*[7,9–11] were also calculated. Examples of the computed non-dimensional longitudinal and vertical velocities $(u_x/(\omega a), u_z/(\omega a))$ and accelerations $(a_x/(\omega^2 a), a_z/(\omega^2 a))$ are shown in Fig. 2 for the most intense wave conditions and two different values of the Stokes number, panels (a)–(d) $S_t = 9 \times 10^{-4}$ and panels (e)–(h) $S_t = 5.77 \times 10^{-2}$. In all cases, the coefficient D was set at $10^{-6}\,m^2\,s^{-1}$. Note that particle variables are drawn in red and *fluid seen by particle* variables in blue.

In all cases, velocities and accelerations tend to decrease oscillating around an asymptotic value. The asymptotic values of the longitudinal velocities and both components of the acceleration tend to zero, as soon as the particles reach a depth where the wave velocity field is no longer felt. The depth at which the wave velocities are zero depends only on the wave parameter,

TABLE I. Wave and particle parameters used for the numerical simulations.

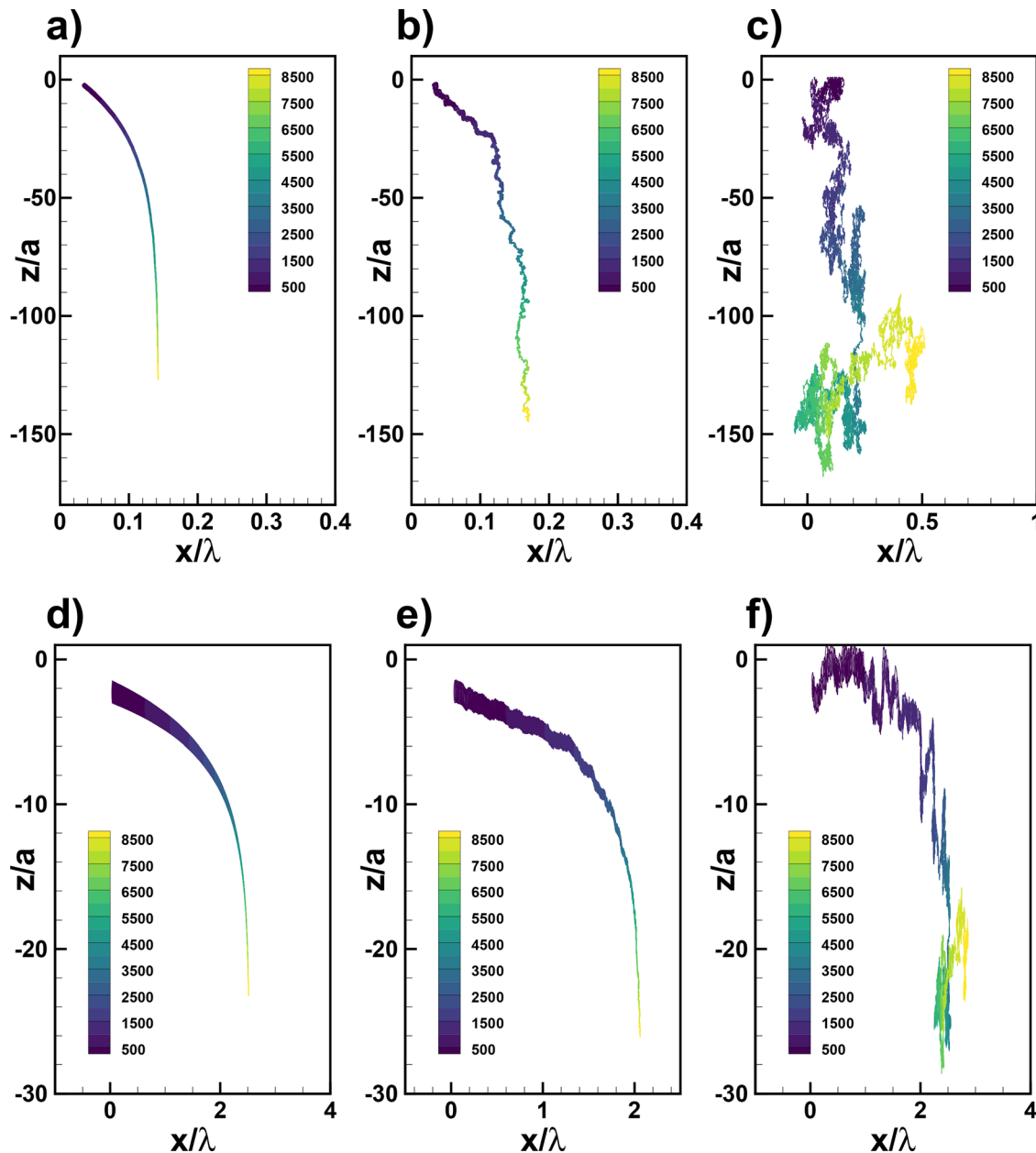| Test No.	d_p (μm)	a (m)	ω (Hz)	H/gT^2	λ (m)	β	τ (s)	S_t	D (m^2/s)	No. sim.
000	100–1000	0.18	1.05	0.001	56.21	0.968	0.000 86–0.086	0.0009–0.09	10^{-6}–10^{-1}	114
001	100–1000	0.36	1.05	0.002	56.21	0.968	0.000 86–0.086	0.0009–0.09	10^{-6}–10^{-1}	114
002	100–1000	0.71	1.05	0.004	56.21	0.968	0.000 86–0.086	0.0009–0.09	10^{-6}–10^{-1}	114
003	100–1000	1.06	1.05	0.006	56.21	0.968	0.000 86–0.086	0.0009–0.09	10^{-6}–10^{-1}	114

FIG. 1. Example of particle trajectories for the same particle, $S_t = 2 \times 10^{-3}$, and different waves and coefficient D. $H/gT^2 = 0.001$: (a) $D = 10^{-6}$; (b) $D = 10^{-3}$; (c) $D = 10^{-1}$ m^2 s^{-1}. $H/gT^2 = 0.006$ (d) $D = 10^{-6}$; (e) $D = 10^{-3}$; (f) $D = 10^{-1}$ m^2 s^{-1}. For all panels, particles have been released in the same position and at the same time. The colors represent the time.

whereas the time at which the particles reach this depth depends on the particle properties. At this depth, heavy particles tend to behave as settling particles in still fluid; thus, their vertical velocity is simply described by the Stokes settling velocity $w_s = -(1 - \beta)g\tau$.[25]

It is worth noting that the vertical velocity of the *fluid seen by particle* tends to zero differently from the particle vertical velocity. This is clearly visible in panel (f), where the vertical velocity of the heavy particle tends to a constant non-zero value (the Stokes settling velocity). Moreover, the random contribution $\sqrt{2D}\mathbf{R}(t)$ modifies the velocities and acceleration at a small Stokes number, see Fig. 2 panels (a)–(d), whereas it is already ineffective for the Stokes number of order 10^{-2}, see panels (e)–(f). For a larger Stokes number, the effect of the stochastic terms is even less important also for the highest value of the coefficient D.
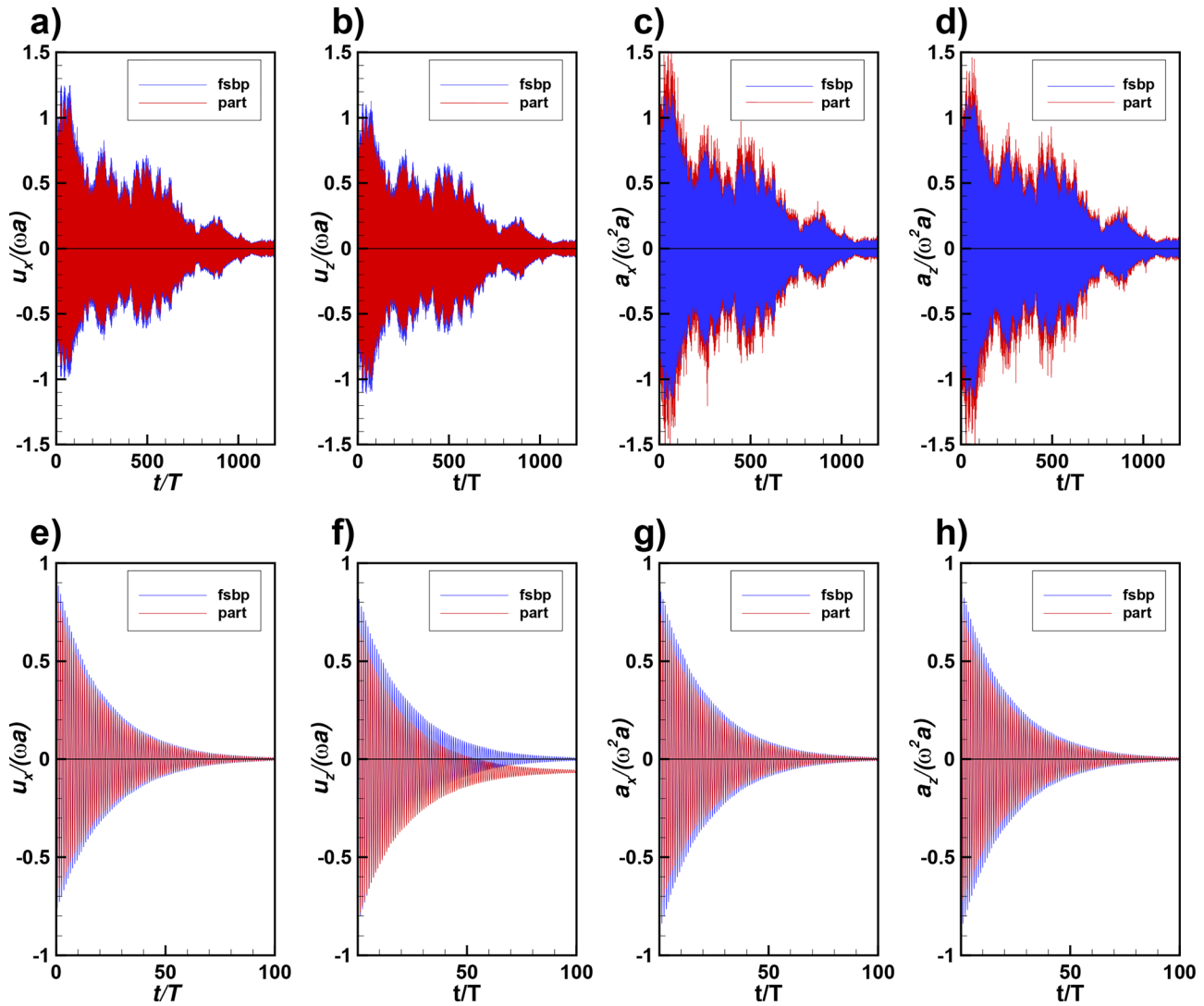
03 February 2025 01:01:57

FIG. 2. Example of non-dimensional velocities and acceleration time signals for two values of the Stokes number and for the same wave parameter $H/gT^2 = 0.006$ and diffusion coefficient ($D = 10^{-3}$ m^2 s^{-1}). Panels (a)–(d) $S_t = 9 \times 10^{-4}$, panels (e)–(h) $S_t = 5.77 \times 10^{-2}$.

B. Lagrangian auto-correlation functions and integral scales

1. Definition of the auto-correlation functions

Starting from the trajectories computed using system (7), we first introduce the Lagrangian auto-correlation functions and, then, we discuss their shapes and integral time scales depending on the main controlling parameters. The knowledge of their shapes is essential to understand the dispersion process.[23]

For a generic variable g, we define the Lagrangian auto-correlation function as $\rho_g(\tau) = \langle g(t)g(t+\tau)\rangle$, where the brackets indicate an ensemble average. Considering, at this moment, the fluid velocities (u_x, u_z) and fluid acceleration (a_x, a_z), we can define the normalized Lagrangian auto-correlation function as

$$R_{u_x}(\tau) = \frac{\rho_{u_x}(\tau)}{\sqrt{\rho_{u_x}(0)\rho_{u_x}(0)}}, \quad R_{u_z}(\tau) = \frac{\rho_{u_z}(\tau)}{\sqrt{\rho_{u_z}(0)\rho_{u_z}(0)}},$$

$$R_{a_x}(\tau) = \frac{\rho_{a_x}(\tau)}{\sqrt{\rho_{a_x}(0)\rho_{a_x}(0)}}, \quad R_{a_z}(\tau) = \frac{\rho_{a_z}(\tau)}{\sqrt{\rho_{a_z}(0)\rho_{a_z}(0)}}. \quad (8)$$

The auto-correlations are then used to evaluate the Lagrangian integral scales T_u as

$$T_{u_x} = \int_0^{+\infty} R_{u_x} d\tau, \quad T_{u_z} = \int_0^{+\infty} R_{u_z} d\tau, \quad T_u = \frac{1}{2}(T_{u_x} + T_{u_z}),$$

$$T_{a_x} = \int_0^{+\infty} R_{a_x} d\tau, \quad T_{a_z} = \int_0^{+\infty} R_{a_z} d\tau, \quad T_a = \frac{1}{2}(T_{a_x} + T_{a_z}). \quad (9)$$

Similarly, we can define the normalized auto-correlation functions and their corresponding integral scales for the particle velocities

03 February 2025 01:01:57

and accelerations (indicated in the following with a superscript p) and the *fluid seen by particle* velocities and acceleration (indicated in the following with a superscript f).

In general, the normalized auto-correlation functions of the fluid, the particle and the *fluid seen by particles* could display a different behavior; note that in the case of a passive tracer (limiting case for mass-less particle) all these quantities collapse together and are equal to the ones calculated for the carrier fluid.

Following Taylor's theory,[22] formulated for tracers, or its recent generalization to different dynamical models for inertial particles,[23] the definition of a diffusion coefficient is inherently related to the finite value of the limit time that tends to infinity of the auto-correlation functions. Thus, a time independent diffusion coefficient requires that the auto-correlation functions decay rapidly in time, regardless if we are considering tracers or inertial particles.

Commonly, the velocity fields used to compute the auto-correlation functions and integral scales are built removing an average component when present. In the present case, no background constant flow is added to the wave field. However, care must be taken when the vertical velocity is considered. In fact, when the particles reach a certain depth, the leading order term in the particle velocity equation, see (7), is the buoyancy term.[25] This term, being independent of time, would produce a spurious effect on the auto-correlation function and, ultimately, a long-time mean square dispersion that grows as time squared. Thus, the $R_{u_z}^p$ has been evaluated subtracting the asymptotic settling velocity reached by the particle when the effects of wave fields are no longer felt, namely $u_z' = u_z - w_s$, where w_s is the Stokes settling velocity.

The integral Lagrangian scales defined above can be considered as an *internal* time scale determined by the dynamic described by system (7), provided the Eulerian velocity field computed with system

(1). In the problem at hand, however, other *external* time scales appear, namely, the wave period T (typical of the fluid flow) and the Stokes time τ (typical of the particle).

The wave periodicity is of particular interest; in fact, the periodicity of the velocity wave field and the resulting Stokes drift is felt also by the particle motion, see Figs. 1 and 2, and its derived properties. The looping character of the particle position and velocity is reflected on a looping-like auto-correlation function. The wave period is the external time scale related to the flow forcing and, not surprisingly, it is reflected in the auto-correlation that assumes a looping shape, whereas this tends to zero.[47]

2. Velocity and acceleration auto-correlation functions of inertial particles and fluid seen by particles

Figure 3 shows the particle horizontal and vertical velocity auto-correlations for the test 000 ($H/gT^2 = 0.001$), and for several Stokes numbers and the extreme values of D, namely 10^{-6} m^2 s^{-1}, panels (a) and (b), and 10^{-1} m^2 s^{-1}, panels (c) and (d).

Although both $R_{u_x}^p$ and $R_{u_z}^p$ tend to zero as time grows, they oscillate around the zero value as shown in the box in panel (b). Comparing panel (a) with (b) and panel (c) with (d), there are no substantial differences between the auto-correlation of the two velocity components. However, we will see in the following that the integral scales show a more marked anisotropy.

Increasing the coefficient D leads to two main effects, see panels (c) and (d): the envelope of the auto-correlation functions tends to zero in shorter times and low frequency oscillations appear. These effects are more clearly visible for low Stokes numbers, whereas higher Stokes numbers are less sensitive to the Gaussian noise. The
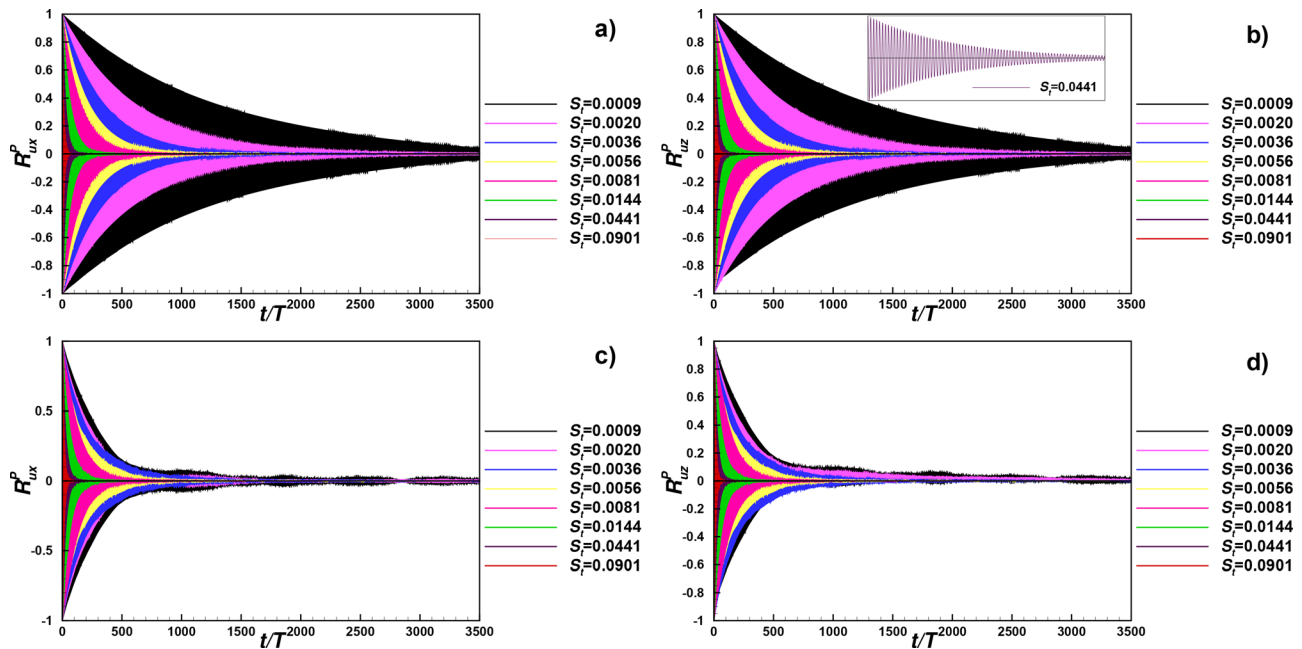

FIG. 3. Normalized velocity auto-correlation for the experiment with $H/gT^2 = 0.001$: (a) $R_{u_x}^p$ with $D = 10^{-6}$ m^2 s^{-1}, b) $R_{u_z}^p$ with $D = 10^{-6}$ m^2 s^{-1}, (c) $R_{u_x}^p$ with $D = 10^{-1}$ m^2 s^{-1}; (d) $R_{u_z}^f$ with $D = 10^{-1}$ m^2 s^{-1}. In panel (b) a zoom in is also inserted to show clearly the looping character of the auto-correlation functions.

appearance of low frequency loops is even more evident with increasing the wave parameter, e.g., for test 003 where the wave parameter has the highest value of the present study ($H/gT^2 = 0.006$), see Fig. 4.

Three values of the Stokes number are reported for the lowest and highest value of the coefficient D. For the case with $S_t = 0.002$, panels (a) and (b), and the case with $S_t = 0.0036$, panels (c) and (d), the vertical auto-correlation shows low frequency loops even with the lowest values of the turbulent diffusion coefficient, whereas for $D = 10^{-1}$ m^2 s^{-1} these lobes are more frequent [panels (b) and (d)].

Differently from previous studies where the vertical velocity auto-correlation increases, reaching almost a constant shape either in the absence of gravity effects[6,7] or when gravity is considered,[19] we found that increasing the Stokes number produces oscillating auto-correlation functions with envelopes that tend to decrease more rapidly to zero. However, the latter aspect will turn out to be misleading in the computation of the integral scales, as discussed in Sec. IV.

Moreover, negative loops are reported by Wang and Stock[19] only in the longitudinal correlation for low or intermediate values of their drift parameters, a measure of the gravity effects compared to the fluid

velocity variance. On the contrary, the vertical correlation calculated by Wang and Stock[19] has a monotonic time decay and increasing values with S_t.

In the present case, the looping character of the auto-correlations does not disappear for increasing Stokes numbers for both directions, $R_{u_x}^p$ and $R_{u_z}^p$.

Regarding the looping character of the auto-correlations, it is interesting to note that the oscillations of the auto-correlation functions occur with a periodicity that does not always coincide with the wave period. Figure 5 shows the cases for the same Stokes number ($S_t = 0.002$) and diffusion coefficient ($D = 10^{-6}$ m^2 s^{-1}) for the different wave conditions. In the figure, the $R_{u_x}^p$ is reported for every instant together with its wave-period sampled value (black line).

For low wave parameters, panel (a), the envelope of the auto-correlation functions coincides with its period-sampled values. Increasing the wave parameter H/gT^2, from panels (b)–(d), the difference between the envelope of the auto-correlation function and its period-sampled value is increasingly noticeable. The non-linear interaction between the typical time scale of the flow and the particle time
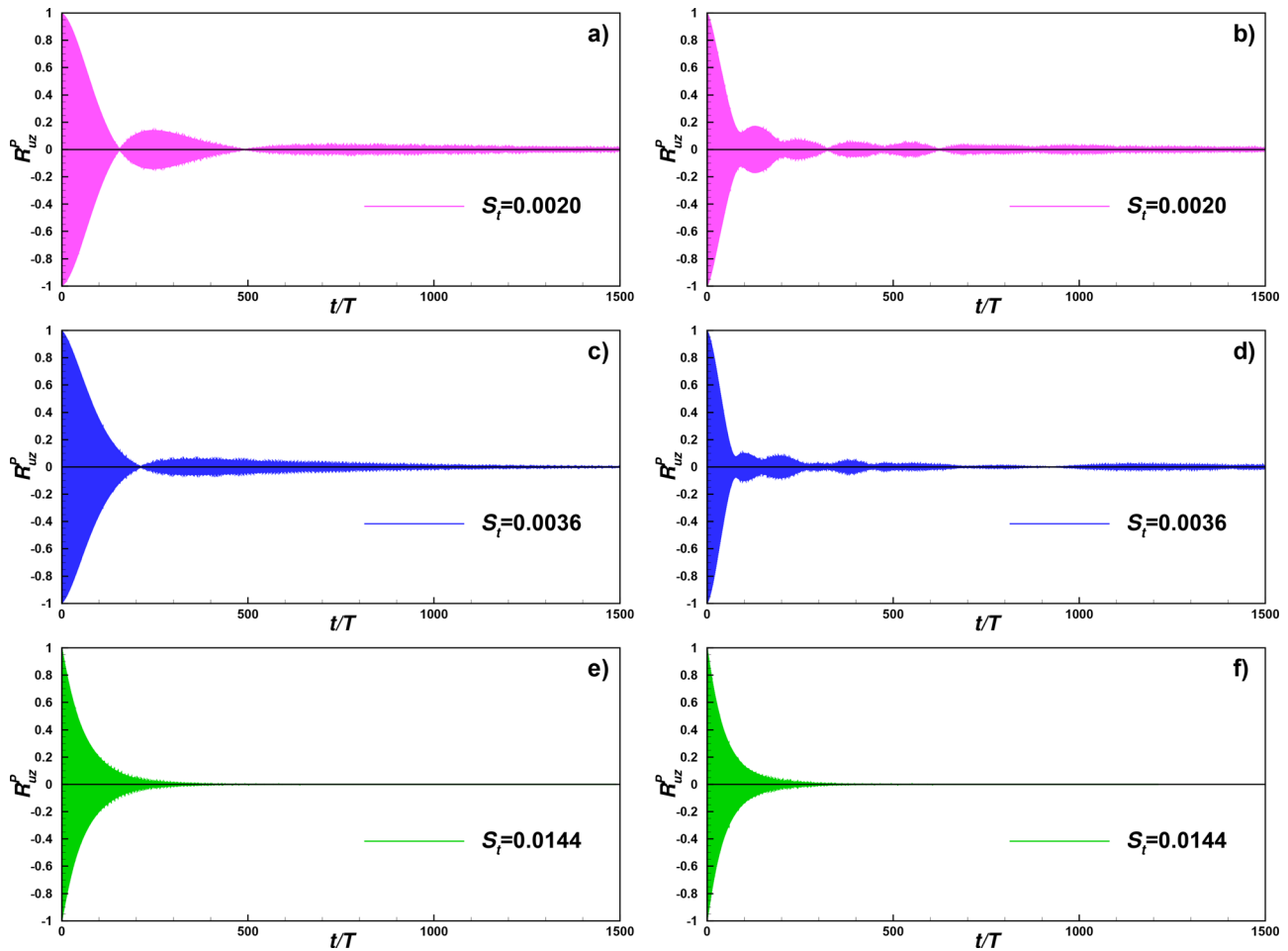

FIG. 4. Normalized vertical velocity auto-correlation $R_{u_z}^p$ for the experiment with $H/gT^2 = 0.006$ with two values of the coefficient D, namely $D = 10^{-6}$ m^2 s^{-1} panels (a), (c), and (e), and $D = 10^{-1}$ m^2 s^{-1} panels (b), (d), and (f), for three values of the Stokes number.
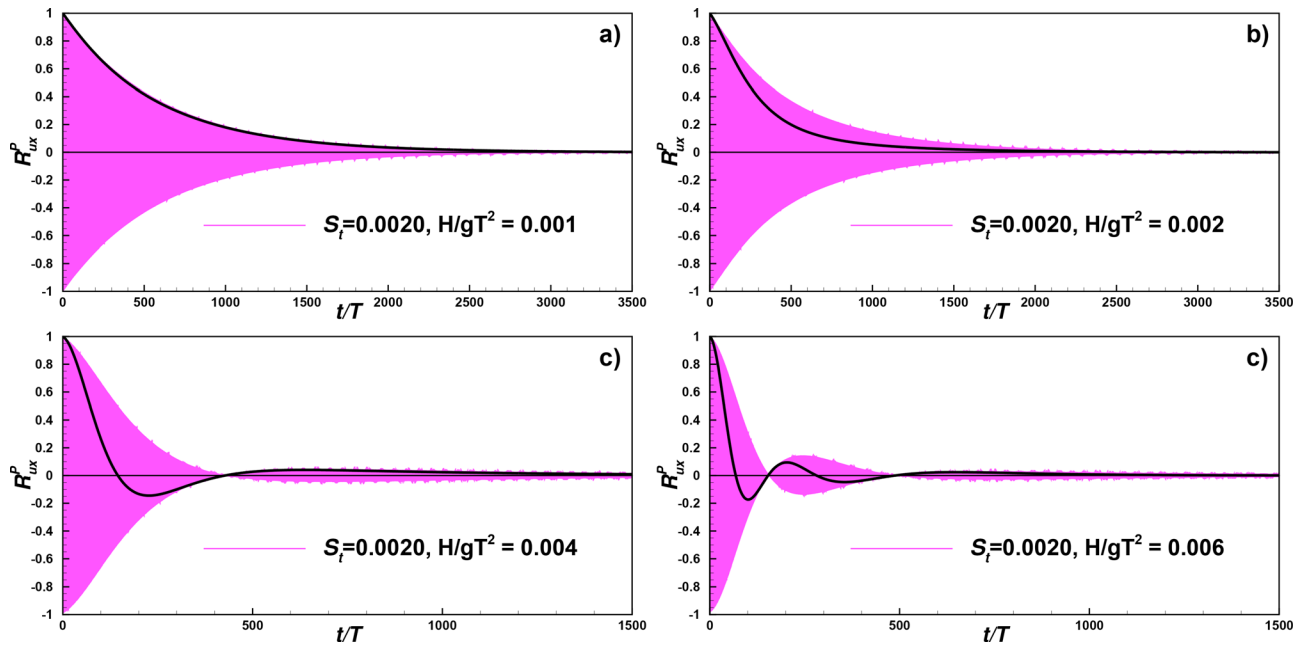
03 February 2025 01:01:57

FIG. 5. Normalized horizontal velocity auto-correlation $R_{u_x}^p$ for all wave conditions, same coefficient $D = 10^{-6}$ m^2 s^{-1} and Stokes number equal to 0.002. Black lines indicate the auto-correlations sampled every period.

scales leads to the generation of oscillations with frequency slower than the forcing wave period. Similar behavior is found for the vertical velocity auto-correlation functions.

If now we compare the correlations of the inertial particles with the *fluid seen by particles*, in all cases the shapes of the auto-correlation functions are extremely similar, whereas we will see that differences are detected in their integral scales.

Finally, no substantial differences in terms of shapes are detected when the acceleration auto-correlation functions are computed.

3. The dependency of the Lagrangian integral time scales on the particle and flow parameters

We now analyze the Lagrangian integral time scales. The complex shapes of the auto-correlation functions and their dependence on S_t and H/gT^2 are reflected on the variability of the integral scales.

Figure 6 summarizes the main findings for the velocity integral scales T_u^p and T_u^f and for the acceleration integral scales T_a^p and T_a^f. Note that the values are normalized with the velocity and acceleration integral scales of the fluid, which assumes values of the order of the wave period T. The different plots correspond to the four values of H/gT^2 and to the two extreme values of the turbulent diffusion, namely, $D = 10^{-6}$ and 10^{-1} m^2 s^{-1}.

Regarding the velocity integral scales of the particle (T_u^p) and of the *fluid seen by particles* (T_u^f), panels (a) and (c), both tend to monotonically decrease for increasing Stokes where $S_t < 10^{-1}$, whereas their trends seem to change for larger values, possibly, indicating an increase for Stokes number that tends to 1.

The effect of the different wave parameters H/gT^2 is again visible for S_t greater than 10^{-1}. In fact, increasing H/gT^2 leads to a more intense wave Stokes drift, owing to its quadratic dependence on the

wave height,[26] and, thus, to a more intense convective transport. The values of T_u^p and T_u^f remain lower than the integral scale of the fluid [i.e., $(T_u^p, T_u^f)/T_u \ll 1$] for the entire range of Stokes number and wave parameters investigated.

Wang and Stock[19] found similar behaviors, in fact, for low S_t the crossing trajectory effects are dominant and yield shorter particle time scales, whereas inertia makes $T_u^p > T_u$ already for $\mathcal{O}(S_t) \sim 1$. In the present case, we did not investigate the regime where $S_t \geq 1$, where we expect the buoyancy terms of system (7) to be dominant and lead to a process close to the standard settling process in still fluid.

As far as the integral velocity time scale for the *fluid seen by particles* T_u^f is concerned, it follows closely the particle counterpart for S_t less than 0.1, especially for high values of the wave parameter. For weak wave $H/gT^2 = 0.001, 0.002$, T_u^f deviates from the particle velocity integral scales and tends to have a non-monotonic dependence on Stokes, with a minimum value around $S_t = 0.25$.

For higher values of the wave parameter, it is reasonably to assume that the higher is the convective velocity (fluid Stokes drift), the closer the particle and its fluid counterparts behave. Moreover, in a wide range of Stokes numbers, the integral velocity scales show a negative power law fitting in the Stokes number of the kind $T_u^p, T_u^f \propto S_t^{-1}$ ($R^2 = 0.99$), see panel (a). The range of validity of the power law increases with higher wave parameters.

The influence of the increased background Gaussian noise contribution is reasonably weak for the range of S_t investigated, see panel (c). In fact, the behavior of both T_u^p and T_u^f is only slightly perturbed even at the maximum value of D.

The monotonic decrease in the particle integral time scale is compatible with the *crossing trajectory effect* described in previous studies
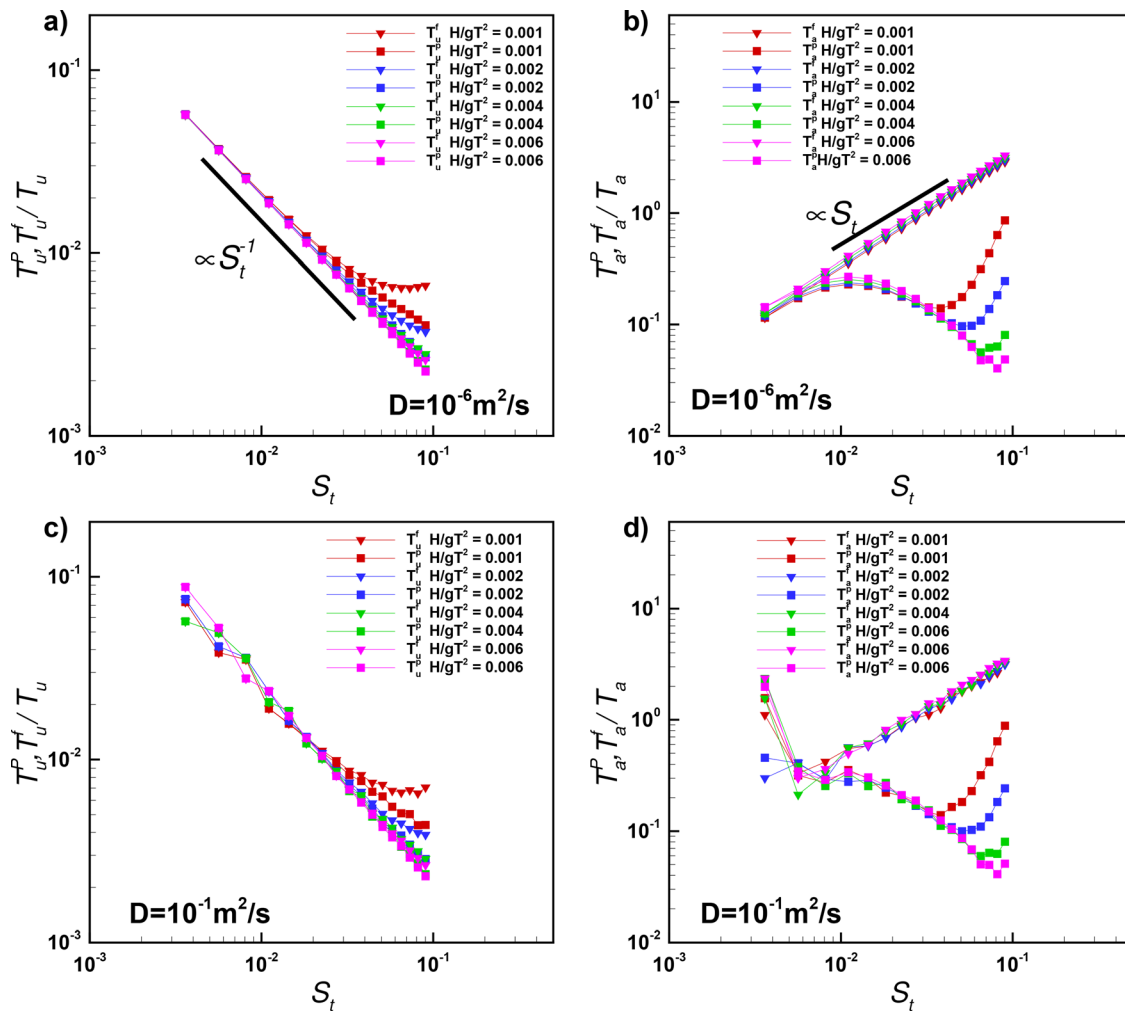
FIG. 6. Normalized integral time scales as a function of S_t for all experiments and for two values of D: (a) velocity integral time scale for $D = 10^{-6}$ m² s⁻¹; (b) acceleration integral time scale for $D = 10^{-6}$ m² s⁻¹; (c) velocity integral time scale for $D = 10^{-1}$ m² s⁻¹; (b) acceleration integral time scale for $D = 10^{-1}$ m² s⁻¹. Square symbols indicate the particle times and the delta symbols the *fluid seen by particle* times.

where gravity effects were included in the description of the transport of inertial particles.[18–20] In fact, for increasing inertia (S_t), the particle trajectories are facilitated to escape from the looping like Eulerian flow structures, typical of the Stokes drift, and loose correlation more rapidly, ultimately, leading to smaller integral time scales. However, we will see in the following that the scales T_u^p and T_u^f, calculated as in equations (9), mask an anisotropic behavior for both the particle and the *fluid seen by particles*.

Accelerations of inertial particles or fluid particles, which are directly related to the wave Stokes drift field, might provide some insight of particle diffusion. Panels (b) and (d) of Fig. 6 report the acceleration integral scales T_a^p and T_a^f. We notice that the particle decorrelation times are no longer monotonic with S_t and less dependent on the wave parameters, except for Stokes numbers greater than 0.1. Moreover, T_a^f seems to be monotonically increasing with the Stokes number following, in this case, a power law of the kind $T_a^f \propto S_t$, with a similar goodness of fitting parameter. As for the velocity integral scales, the *fluid seen by particle* does not show any dependence on H/gT^2.

Contrary to the velocity integral scales, T_a^p is strongly modified by the background turbulence at least for $S_t < 0.03$, increasing the distance with T_a^f. At low levels of Brownian background and for $S_t < 0.05$, in fact, T_a^p and T_a^f are very close to each other. The intermediate decrease in T_a^p is probably due to the deviation of inertial particles from the swirling motion associated with the fluid Stokes drift as the particle inertia increases. As S_t increases further, the particle path becomes insensitive to the flow structure; thus, the integral scales increase owing to the increase in the particle inertia.

Finally, in Fig. 7 we show the variation of the velocity and acceleration components of the particle and *fluid seen by particle* integral scales for two values of the diffusion coefficient D and for two wave conditions, namely, $H/gT^2 = 0.001$, panels (a)–(d) and $H/gT^2 = 0.006$ (e)–(h).
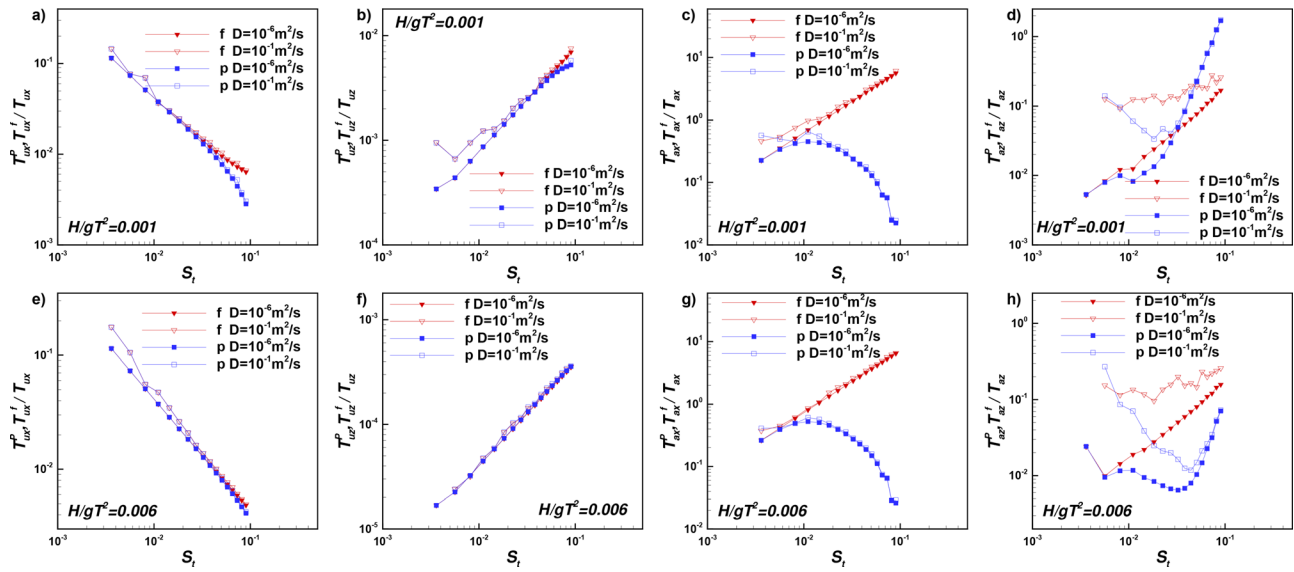
FIG. 7. Velocity and acceleration integral scales for the single x and z components for two values of the diffusion coefficient D and for two wave conditions: (a)–(d) $H/gT^2 = 0.001$; (e)–(h) $H/gT^2 = 0.006$. p in the legend indicates particle integral scales and f indicates *fluid seen by particle*.

Regarding the velocity integral scales, a similar behavior is found regardless of the wave parameters and the diffusion coefficient, and it indicates a strong anisotropy between the longitudinal component T_{ux}^p and the vertical component T_{uz}^p. In fact, the vertical velocity time scale T_{uz}^p tends to increase with the Stokes number. However, its values are always less than the horizontal velocity time scale T_{ux}^p, thus, leading to the overall decay shown in Fig. 6 panels (a) and (c).

The strong similarity between the particle time scales and the *fluid seen by particle* ones is further confirmed, and also the *fluid seen by particle* time scales show the same anisotropy.

The acceleration scales for both the particle and the *fluid seen by particle* show the greatest variability, especially in the vertical direction, see panels (d) and (h), where T_{az}^p and T_{az}^f are plotted. The vertical acceleration time scale seems to be very sensitive to the wave conditions and to the background Brownian noise, whereas its horizontal counterpart is much less influenced. It is indeed the rapid increase in T_{az}^p for Stokes greater than 0.1 that governs the overall trend shown in six panels (b) and (d), reaching also values larger than the fluid particle integral scale.

C. Dispersion regimes

We are now interested in evaluating how the shape of the auto-correlation functions and the variability of the integral scales might influence the dispersion of heavy particles in the present flow conditions.

First, we define the absolute dispersion of the heavy particles $d^2(t)$ as the ensemble average of the particle displacements with respect to an initial position, as the classical definition of Taylor's theory. Assuming to deal with a certain number of particle trajectories released at some initial time t_0, the computation of the absolute dispersion could be performed accounting for or not the displacement of the center of mass of the considered ensemble of particles. In case where

the mean drift of the center of mass is not considered, only the initial particle conditions are relevant, and this strategy has been applied in several geophysical contexts, see Refs. 48–51 among others.

A different approach in the evaluation of the absolute dispersion involves the computation of a mean drift related to the center of mass of a cluster of particles.[48,51] The total absolute dispersion is, therefore, evaluated removing at each time the position of the center of mass, and the dispersion coefficient is simply the time derivative of $d^2(t)$.

For the present analysis, we preferred to use this second strategy of computation, which allows for an immediate removal of spurious effects to mean drift that might lead to artifacts in the total dispersion.

It is worth recalling that Taylor[22] found that for times smaller than the Lagrangian time scale a square time dependence of the absolute dispersion is recovered, i.e., $d^2(t) = \rho(0)t^2$, whereas for times greater than T^L a linear dependence in time is found $[d^2(t) = 2\rho(0)T^L t + \text{const}]$. The latter implies the existence of diffusive (Brownian) regime characterized by a diffusion coefficient expressed as $K = \rho(0)T^L$. These two regimes, originally derived for fluid particles, have been found to be formally valid also for inertial particles[6,7,18,23] and the existence of the diffusive regimes has been widely investigated in different contexts, owing to its extreme practical importance.

Taking advantage of the definition of K, several authors inferred the value of the coefficient providing a model for the particle velocity integral scale and, most of the time, comparing the value to the fluid value.

In the present case, the behavior of the non-dimensional absolute dispersion d^2/λ^2 is affected by the combined effect of different time scales: the wave period, the convective time scale corresponding to the wave Stokes drift, the Stokes time and the integral time scales.

Figure 8 panel (a) shows the total absolute dispersion normalized by the wavelength d^2/λ^2, vs the dimensionless time t/T. The oscillating character, imposed by the periodic Eulerian velocity field, is observed also in the time evolution of d^2/λ^2, similarly to the auto-correlation
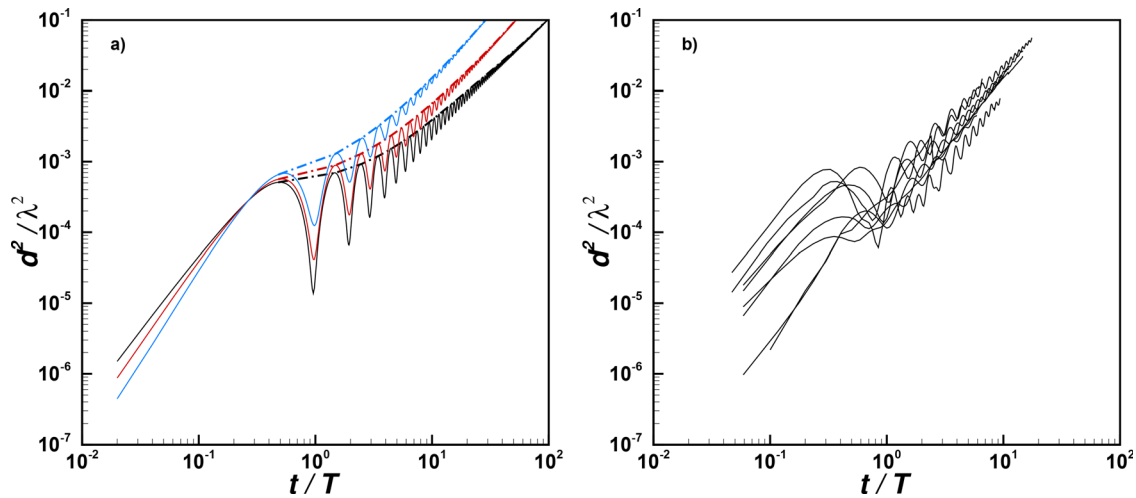
FIG. 8. Non-dimensional absolute dispersion d^2/λ^2 as a function of non-dimensional time t/T. (a) Results for $H/gT^2 = 0.004$ and three values of the Stokes number $S_t = 0.022, 0.044,$ and 0.081. (b) Non-dimensional absolute dispersion estimated from the experiments by De Leo et al.[29] for similar wave and particle parameters.

functions. The periodicity is well captured by the choice of T as the time scale for the non-dimensional time. In panel (a), we also report the values of d^2/λ^2 sampled every wave period, i.e., retaining just the oscillation peaks (dot dashed-lines), which will help in describing the dispersion regimes. Panel (b) shows d^2/λ^2 evaluated from the experiments presented in De Leo et al.[29] with similar wave and particle parameters for comparison. A similar oscillating total absolute dispersion is recovered also in the experiments.

Figure 9 shows wave period sampled d^2/λ^2 varying H/gT^2, for three different values of the Stokes number, $S_t = 0.0009, 0.027,$ and 0.09.

The green solid line represents the ballistic regime, $d^2/\lambda^2 \propto (t/T)^2$, whereas the red solid line represents the diffusive regime $d^2/\lambda^2 \propto (t/T)$. Moreover, for the same S_t, we report the results obtained with three values of the turbulent diffusion D. For the case $H/gT^2 = 0.004$, panel (c), the non-dimensional absolute dispersion computed starting from the observed particle trajectories during the experiments[29] is also reported for comparison. The experimental non-dimensional absolute dispersion follows closely the ballistic regime, and its values correctly fall between the two numerical simulations for the Stokes number equal to 0.027 and 0.09. A first important observation is that no asymptotic diffusive regime exists in the range of parameters investigated (wave and particle parameters) with very few exceptions. This is in contrast with what has been observed in other contexts of diffusion of heavy particles. In fact, a Brownian regime was observed already in the seminal paper by Csanady,[18] who retained the gravity effect in his theory, claiming a difference between particle diffusion and fluid diffusion coefficient owing to crossing trajectories effect and continuity effect.

Moreover, the existence of a diffusion regime for heavy particles in turbulent flows without gravity effect or added-mass effect was always reported even for much higher Stokes numbers.[6,7] Depending on the value of the Stokes number, the diffusion coefficient could also be increased by inertial effect, leading to values of the particle Schmidt number (ratio between particle long-time diffusion over fluid diffusion) between 0.1 and 2.

The present results, instead, show that a linear dependence of the absolute dispersion appears as a transient regime, only at a very low Stokes number, between two quadratic regimes. Not surprisingly, a linear regime could be also recovered for very low values of the Stokes number and wave parameter and with a fairly high value of the Brownian process coefficient D of the order of 10^{-3} m^2 s^{-1} or higher. However, as soon as S_t is greater than 0.002, the only regime clearly visible is the quadratic one. As the wave parameter increases, i.e., the wave Stokes drift is more intense, the behavior of all particles tends to collapse to very similar values, see panel (d).

The generalization of Taylor's theory has been described by Boi et al.[23] for several inertial forces, and the buoyancy-forced case is particularly relevant for the present study. The asymptotic diffusion coefficient can be defined, and it requires that the integral of the particle auto-correlation converges to a finite value. Superdiffusive regimes, as the ballistic here described, are associated with a non-convergent integral owing to a slowly decaying correlation, i.e., a long integral scale.

In the present case, the integral time scales, presented in Fig. 6, show finite values; however, the shape of the correlation functions might be responsible for the disappearance of the Brownian regime. A possible physical explanation of the present results could be found in the settling process of heavy particles. The trajectory followed by the heavy particle could resemble the behavior described through the crossing trajectory effect introduced by Yudine[17] and Csanady[18] and resumed by Shao[20] and Jung et al.[7] Moreover, Santamaria et al.[25] already demonstrated with a simple monochromatic wave that the net settling velocity is increased by the interplay of the wave Stokes drift and the particle inertia. This was further confirmed numerically by Stocchino et al.[27] and experimentally by De Leo et al.[29] The particle exits the fluid trajectory owing to inertial and gravity effect with an increased settling velocity, whereas it continues to be correlated and anti-correlated over a long time period.

Similar results are found by DiBenedetto, Ouellette, and Koseff[26] for the longitudinal dispersion and it was described as the settling regime. In other contexts, *superdiffusion processes* were associated with
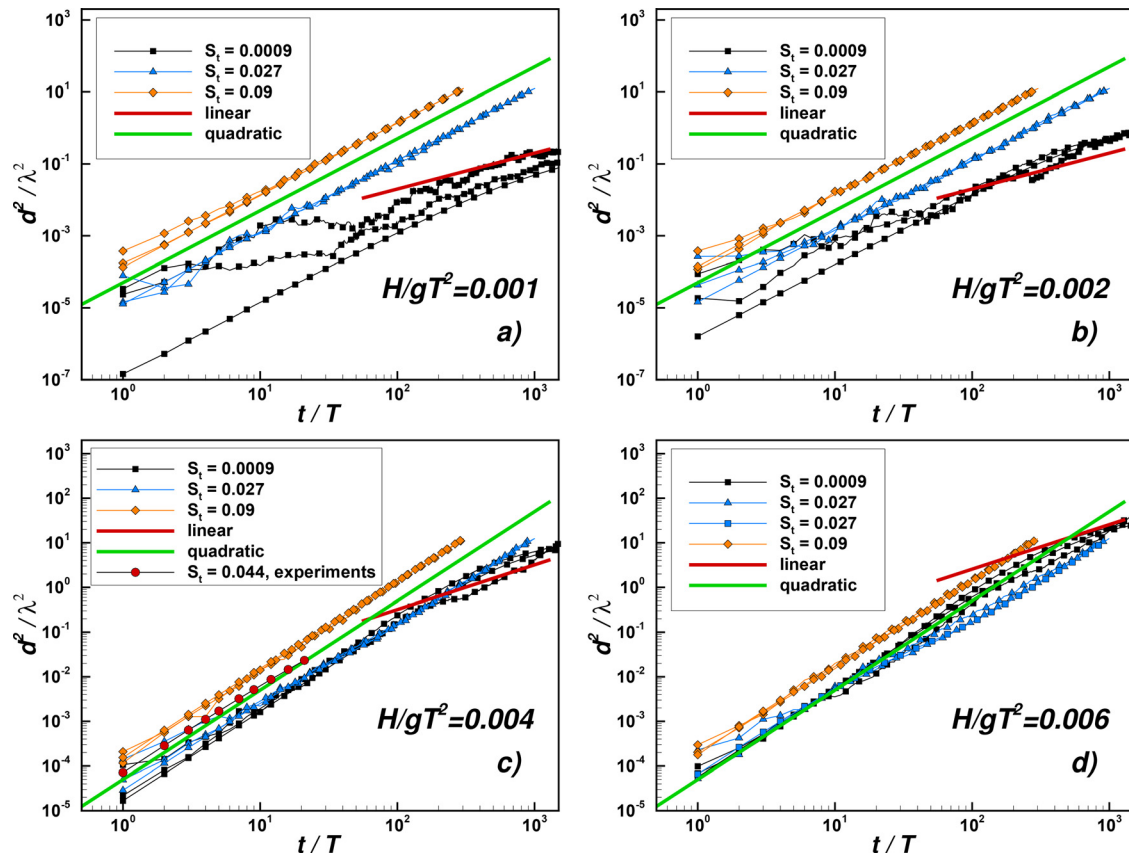
FIG. 9. Normalized absolute dispersion for different wave parameters, Stokes number, and turbulent diffusion. For each S_t three curves are plotted for $D = 10^{-6}, 10^{-3}$, and 10^{-1} m^2 s^{-1}. The green solid lines indicates $d^2/\lambda^2 \propto (t/T)^2$ whereas the red solid line stands for $d^2/\lambda^2 \propto (t/T)$.

an overall auto-correlation function that exhibits a strong oscillation pattern, with a significant positive lobe that is more pronounced than the first negative lobe. The associated eddy dispersion was found to be faster than the typical diffusive spreading.[52,53] In the cited studies, the looping like auto-correlation was generated by the presence of coherent rotational flow structures that tended to maintain a positive and negative correlation over time, whereas the overall auto-correlation function decreased to zero. Anomalous diffusion regimes were also extensively studied[54] and linked to very strong correlations, which is the condition found in the present case.

IV. CONCLUSIONS

Sea waves generate a net Lagrangian transport by the Stokes drift, which is considered an important source of mass transport in coastal areas. We investigate the wave induced transport of heavy plastics, owing to their environmental importance, and discuss the possibility of the existence of an asymptotic diffusive regime. The present study is relevant in the understanding of microplastic transport models. In fact, among the different classes of plastic debris, particles with size smaller than a millimeter with a density higher than water are commonly observed.[33]

Most of the current numerical transport models (Eulerian or Lagrangian) disregard the inertial character of the microplastic

particles and assume that it is possible to describe the fluxes of plastic particles in terms of an effective dispersion coefficient, implicitly assuming the existence of a diffusive regime.[36,55,56]

On the contrary, the results of the present numerical simulations, performed using a wide range of the main parameters (waves and particles), show that, even for low Stokes numbers ($S_t < 0.36$), no asymptotic diffusive regime is observed except as a transient regime. The dispersion process remains always confined to a ballistic regime.

The effect of an added transport due to a background turbulence is also ineffective, even for the turbulent diffusion coefficient of the order of 10^{-1} m^2 s^{-1}, except for a very low value of the Stokes number ($S_t < 0.005$) and wave parameter.

Heavy particles under the action of wave transport behave very differently from fluid particles showing correlations and integral scales far from the ones valid for passive particles. The looping like auto-correlations strongly influence the dispersion processes, inhibiting the establishment of a diffusive process following the classical Taylor's law. This conclusion is further demonstrated by the behavior of the absolute dispersion obtained from measured particle trajectories.

Note that the range of parameters investigated well represents the observations of microplastic in marine environment in terms of typical values of β and S_t.[33] Therefore, we question the adoption of a Fickian-like law to model the fluxes of heavy particles, which requires

03 February 2025 01:01:57

a diffusive regime for time longer than the fluid integral time scale. Thus, a more refined transport model would be required to correctly simulate the fate of heavy particles in coastal and open ocean circulations.

Several aspects need to be further investigated such as the role of a wave spectrum instead of a regular wave Eulerian field, a random distribution of particles described as a cluster and a more realistic non-spherical shape.

ACKNOWLEDGMENTS

AUTHOR DECLARATIONS
Conflict of Interest

The authors have no conflicts of interest to disclose.

DATA AVAILABILITY

The data that support the findings of this study are available from the corresponding author upon reasonable request.

REFERENCES

[1] J. Bec, L. Biferale, G. Boffetta, A. Celani, M. Cencini, A. Lanotte, S. Musacchio, and F. Toschi, "Acceleration statistics of heavy particles in turbulence," J. Fluid Mech. **550**, 349–358 (2006).

[2] J. Bec, L. Biferale, M. Cencini, A. Lanotte, S. Musacchio, and F. Toschi, "Heavy particle concentration in turbulence at dissipative and inertial scales," Phys. Rev. Lett. **98**, 084502 (2007).

[3] M. Cencini, J. Bec, L. Biferale, G. Boffetta, A. Celani, A. Lanotte, S. Musacchio, and F. Toschi, "Dynamics and statistics of heavy particles in turbulent flows," J. Turbul. **7**, N36 (2006).

[4] S. Ayyalasomayajula, A. Gylfason, L. R. Collins, E. Bodenschatz, and Z. Warhaft, "Lagrangian measurements of inertial particle accelerations in grid generated wind tunnel turbulence," Phys. Rev. Lett. **97**, 144507 (2006).

[5] S. Gerashchenko, N. Sharp, S. Neuscamman, and Z. Warhaft, "Lagrangian measurements of inertial particle accelerations in a turbulent boundary layer," J. Fluid Mech. **617**, 255 (2008).

[6] S. Wetchagarun and J. J. Riley, "Dispersion and temperature statistics of inertial particles in isotropic turbulence," Phys. Fluids **22**, 063301 (2010).

[7] J. Jung, K. Yeo, and C. Lee, "Behavior of heavy particles in isotropic turbulence," Phys. Rev. E **77**, 016307 (2008).

[8] Q. Zhang and Z. Xiao, "Single-particle dispersion in compressible turbulence," Phys. Fluids **30**, 040904 (2018).

[9] J. Pozorski and J.-P. Minier, "On the Lagrangian turbulent dispersion models based on the Langevin equation," Int. J. Multiphase Flow **24**, 913–945 (1998).

[10] J. Pozorski and J.-P. Minier, "Probability density function modeling of dispersed two-phase turbulent flows," Phys. Rev. E **59**, 855 (1999).

[11] Z. He, Z. Liu, S. Chen, L. Weng, and C. Zheng, "Direct numerical simulation of particle behavior in homogeneous isotropic turbulence," J. Chem. Ind. Eng. **2**, 167–188 (2006).

[12] P. Weiss, D. Oberle, D. W. Meyer, and P. Jenny, "Impact of turbulence forcing schemes on particle clustering," Phys. Fluids **31**, 061703 (2019).

[13] K. O. Fong, O. Amili, and F. Coletti, "Velocity and spatial distribution of inertial particles in a turbulent channel flow," J. Fluid Mech. **872**, 367–406 (2019).

[14] A. Barge and M. Gorokhovski, "Acceleration of small heavy particles in homogeneous shear flow: Direct numerical simulation and stochastic modelling of under-resolved intermittent turbulence," J. Fluid Mech. **892**, A28 (2020).

[15] T. Berk and F. Coletti, "Dynamics of small heavy particles in homogeneous turbulence: A Lagrangian experimental study," J. Fluid Mech. **917**, A47 (2021).

[16] L. J. Baker and F. Coletti, "Particle-fluid-wall interaction of inertial spherical particles in a turbulent boundary layer," J. Fluid Mech. **908**, A39 (2021).

[17] M. Yudine, "Physical considerations on heavy-particle diffusion," in *Advances in Geophysics* (Elsevier, 1959), Vol. 6, pp. 185–191.

[18] G. Csanady, "Turbulent diffusion of heavy particles in the atmosphere," J. Atmos. Sci. **20**, 201–208 (1963).

[19] L.-P. Wang and D. E. Stock, "Dispersion of heavy particles by turbulent motion," J. Atmos. Sci. **50**, 1897–1913 (1993).

[20] Y.-P. Shao, "A Lagrangian stochastic model for nonpassive particle diffusion in turbulent flows," Math. Comput. Model. **21**, 31–37 (1995).

[21] K. Gustavsson and B. Mehlig, "Statistical models for spatial patterns of heavy particles in turbulence," Adv. Phys. **65**, 1–57 (2016).

[22] G. Taylor, "Diffusion by continuous movement," Proc. London Math. Soc. **20**, 196–212 (1921).

[23] S. Boi, A. Mazzino, P. Muratore-Ginanneschi, and S. Olivieri, "Generalization of Taylor's formula to particles of arbitrary inertia," Phys. Rev. Fluids **3**, 104501 (2018).

[24] M. Maxey and J. Riley, "Equation of motion for a small rigid sphere in a nonuniform flow," Phys. Fluids **26**, 883–889 (1983).

[25] F. Santamaria, G. Boffetta, M. M. Afonso, A. Mazzino, M. Onorato, and D. Pugliese, "Stokes drift for inertial particles transported by water waves," Europhys. Lett. **102**, 14003 (2013).

[26] M. H. DiBenedetto, N. T. Ouellette, and J. R. Koseff, "Transport of anisotropic particles under waves," J. Fluid Mech. **837**, 320–340 (2018).

[27] A. Stocchino, F. D. Leo, and G. Besio, "Sea waves transport of inertial microplastics: Mathematical model and applications," J. Mar. Sci. Eng. **7**, 467 (2019).

[28] P. L. Forsberg, D. Sous, A. Stocchino, and R. Chemin, "Behaviour of plastic litter in nearshore waters: First insights from wind and wave laboratory experiments," Mar. Pollut. Bull. **153**, 111023 (2020).

[29] A. De Leo, L. Cutroneo, D. Sous, and A. Stocchino, "Settling velocity of microplastics exposed to wave action," J. Mar. Sci. Eng. **9**, 142 (2021).

[30] V. Hidalgo-Ruz, L. Gutow, R. C. Thompson, and M. Thiel, "Microplastics in the marine environment: A review of the methods used for identification and quantification," Environ. Sci. Technol. **46**, 3060–3075 (2012).

[31] K. L. Law, "Plastics in the marine environment," Annu. Rev. Mar. Sci. **9**, 205–229 (2017).

[32] S. Rezania, J. Park, M. F. M. Din, S. M. Taib, A. Talaiekhozani, K. K. Yadav, and H. Kamyab, "Microplastics pollution in different aquatic environments and biota: A review of recent studies," Mar. Pollut. Bull. **133**, 191–208 (2018).

[33] M. Kooi and A. A. Koelmans, "Simplifying microplastic via continuous probability distributions for size, shape, and density," Environ. Sci. Technol. Lett. **6**, 551–557 (2019).

[34] M. Kooi, E. H. V. Nes, M. Scheffer, and A. A. Koelmans, "Ups and downs in the ocean: Effects of biofouling on vertical transport of microplastics," Environ. Sci. Technol. **51**, 7963–7971 (2017).

[35] J. A. Tesán Onrubia, K. Djaoudi, F. Borgogno, S. Canuto, B. Angeletti, G. Besio, M. Capello, L. Cutroneo, A. Stocchino, S. Mounier *et al.*, "Quantification of microplastics in north-western Mediterranean harbors: Seasonality and biofilm-related metallic contaminants," J. Mar. Sci. Eng. **9**, 337 (2021).

[36] A. Isobe, K. Kubo, Y. Tamura, E. Nakashima, N. Fujii *et al.*, "Selective transport of microplastics and mesoplastics by drifting in coastal waters," Mar. Pollut. Bull. **89**, 324–330 (2014).

[37] I. Jalón-Rojas, X.-H. Wang, and E. Fredj, "On the importance of a three-dimensional approach for modelling the transport of neustic microplastics," Ocean Sci. **15**, 717–724 (2019).

[38] M. Reeks, "The relationship between Brownian motion and the random motion of small particles in a turbulent flow," Phys. Fluids **31**, 1314–1316 (1988).

[39] M. Rosti, S. Olivieri, M. Cavaiola, A. Seminara, and A. Mazzino, "Fluid dynamics of COVID-19 airborne infection suggests urgent data for a scientific design of social distancing," Sci. Rep. **10**, 22426 (2020).

[40] R. G. Dean and R. A. Dalrymple, *Water Wave Mechanics for Engineers and Scientists* (World Scientific Publishing Company, 1991), Vol. 2.

[41] D. Peregrine, "Interaction of water waves and currents," in *Advances in Applied Mechanics* (Elsevier, 1976), Vol. 16, pp. 9–117.

[42] S. Boi, M. M. Afonso, and A. Mazzino, "Anomalous diffusion of inertial particles in random parallel flows: Theory and numerics face to face," J. Stat. Mech. **2015**, P10023.

[43]E. Van Sebille, S. M. Griffies, R. Abernathey, T. P. Adams, P. Berloff, A. Biastoch, B. Blanke, E. P. Chassignet, Y. Cheng, C. J. Cotter *et al.*, "Lagrangian ocean analysis: Fundamentals and practices," Ocean Modell. **121**, 49–75 (2018).

[44]Y. Drossinos and M. W. Reeks, "Brownian motion of finite-inertia particles in a simple shear flow," Phys. Rev. E **71**, 031113 (2005).

[45]S. Boi, A. Mazzino, and G. Lacorata, "Explicit expressions for eddy-diffusivity fields and effective large-scale advection in turbulent transport," J. Fluid Mech. **795**, 524–548 (2016).

[46]L. Khatmullina and I. Isachenko, "Settling velocity of microplastic particles of regular shapes," Mar. Pollut. Bull. **114**, 871–880 (2017).

[47]M. Farazmand and T. Sapsis, "Surface waves enhance particle dispersion," Fluids **4**, 55 (2019).

[48]J. LaCasce, "Statistics from Lagrangian observations," Prog. Oceanogr. **77**, 1–29 (2008).

[49]A. Stocchino, G. Besio, S. Angiolani, and M. Brocchini, "Lagrangian mixing in straight compound channels," J. Fluid Mech. **675**, 168–198 (2011).

[50]A. J. Mariano, E. Ryan, H. Huntley, L. Laurindo, E. Coelho, A. Griffa, T. Özgökmen, M. Berta, D. Bogucki, S. S. Chen *et al.*, "Statistical properties of the surface velocity field in the northern Gulf of Mexico sampled by glad drifters," J. Geophys. Res. **121**, 5193–5216, https://doi.org/10.1002/2015JC011569 (2016).

[51]F. Enrile, G. Besio, A. Stocchino, and M. G. Magaldi, "Influence of initial conditions on absolute and relative dispersion in semi-enclosed basins," PLoS One **14**, e0217073 (2019).

[52]P. S. Berloff, J. C. McWilliams, and A. Bracco, "Material transport in oceanic gyres. Part i: Phenomenology," J. Phys. Oceanogr. **32**, 764–796 (2002).

[53]M. Veneziani, A. Griffa, A. M. Reynolds, and A. J. Mariano, "Oceanic turbulence and stochastic models from subsurface Lagrangian data for the northwest Atlantic Ocean," J. Phys. Oceanogr. **34**, 1884–1906 (2004).

[54]P. Castiglione, A. Mazzino, P. Muratore-Ginanneschi, and A. Vulpiani, "On strong anomalous diffusion," Physica D **134**, 75–93 (1999).

[55]H. Zhang, "Transport of microplastics in coastal seas," Estuarine, Coastal Shelf Sci. **199**, 74–86 (2017).

[56]E. Van Sebille, S. Aliani, K. L. Law, N. Maximenko, J. M. Alsina, A. Bagaev, M. Bergmann, B. Chapron, I. Chubarenko, A. Cózar *et al.*, "The physical oceanography of the transport of floating marine debris," Environ. Res. Lett. **15**, 023003 (2020).

03 February 2025 01:01:57